Perturbation-Specific Transcriptional Mapping facilitates unbiased target elucidation of antibiotics.

Keith P Romano[a,b,c,1]
Josephine Bagnall[a,1]
Thulasi Warrier[a,b,2]
Jaryd Sullivan[a,b,d,2]
Kristina Ferrara[a,b]
Marek Orzechowski[e]
Phuong H Nguyen[a,b,d]
Kyra Raines[a,b]
Jonathan Livny[a]
Noam Shoresh[a]
Deborah T Hung[a,b,d,3]

[a]*The Broad Institute of MIT and Harvard, Cambridge, Massachusetts, USA*
[b]*Center for Computational and Integrative Biology, Massachusetts General Hospital, Boston, Massachusetts, USA*
[c]*Division of Pulmonary and Critical Care Medicine, Brigham and Women's Hospital, Boston Massachusetts, USA*
[d]*Department of Genetics, Harvard Medical School, Boston, Massachusetts, USA*

[1]*KPR. and JB contributed equally to this work.*
[2]*TW and JS contributed equally to this work.*
[3]*To whom correspondence may be addressed. Email: hung@molbio.mgh.harvard.edu*

Author Contributions: KPR designed and performed gene expression experiments with the assistance of TW, JS, KF, PHN. and KR. JB performed the data analysis with the assistance of MO and NS. KPR, TW, JS and KF constructed all strains used in this study. JS performed DNA gyrase-related experiments. KPR wrote the manuscript in consultation with JB, TW, JS, JL, NS and DTH.

Competing Interest Statement: The authors declare no competing interests.

Classification: Biological Sciences, Microbiology

Keywords: Transcriptomics, RNA-Seq, Pseudomonas, antibiotics, mechanism-of-action

This PDF file includes:
Main Text
Figures 1 to 3
Tables 1 to 3

Abstract

The rising prevalence of antibiotic resistance threatens human health. While more sophisticated strategies for antibiotic discovery are being developed, target elucidation of new chemical entities remains challenging. In the post-genomic era, expression profiling can play an important role in mechanism-of-action (MOA) prediction by reporting on the cellular response to perturbation. However, the broad application of transcriptomics has yet to fully fulfill its promise of transforming target elucidation. We developed an unbiased strategy for MOA prediction, called Perturbation-Specific Transcriptional Mapping (PerSpecTM), in which large-throughput expression profiling of wild-type or hypomorphic mutants depleted for essential targets, enables a reference-based strategy to associate similar perturbations, whether small molecule or genetic, based on the principle that similar perturbations will elicit similar transcriptional responses. We applied this approach to rapidly elucidate the MOAs of three new molecules with activity against the important bacterial pathogen *Pseudomonas aeruginosa* by mapping their expression profiles to those generated for a reference set of antimicrobial compounds with known MOA. Meanwhile, we also show that small molecule inhibition can be mapped to genetic depletion of essential targets by CRISPRi by PerSpecTM, thus demonstrating proof-of-concept that correlations between expression profiles of small molecule and genetic perturbations can predict MOA when no chemical entities exist to serve as a reference. Empowered by PerSpecTM and its leveraging of reference transcriptional profiles for known small molecule or genetic perturbations, this work lays the foundation for an unbiased, readily scalable, systematic reference-based strategy for MOA elucidation that could transform antibiotic discovery efforts.

60 **Significance Statement**

61 In an era of increasing antibiotic resistance, new antibiotics are critically needed. However, MOA elucidation remains
62 a challenging step in antibiotic discovery and thus a major bottleneck. Building on the principle that molecules with
63 similar MOAs elicit similar transcriptional responses, we have now developed a highly scalable strategy for MOA
64 prediction in the important bacterial pathogen *Pseudomonas aeruginosa* based on correlations between the
65 expression profiles of new molecules and known perturbations, either small molecule inhibition by known antibiotics or
66 transcriptional repression of essential targets by CRISPRi. By rapidly assigning MOA to three new molecules with
67 anti-pseudomonal activity, we provide proof-of-concept for a rapid, comprehensive, systematic, reference-based
68 approach to MOA prediction, with the potential to transform antibiotic discovery efforts.

Main Text

Introduction

Pseudomonas aeruginosa and other gram-negative bacteria pose a major threat to human health due to the growing prevalence of antibiotic resistance in healthcare settings. Surging multi-drug-resistant bacterial infections threaten to outpace our ability to develop novel antibiotics[1-4]. Antibiotic discovery campaigns have failed to deliver new antibiotic classes, including extensive efforts in the post-genomic era. As recently reviewed, new strategies are being developed to address the looming antibiotic shortage through target-based approaches carried out in whole cells at scale[5]. Most of these novel approaches differ from standard target-based screening, in which the target is known by design, because they prioritize the identification of new molecules with whole-cell antibacterial activity. For example, in a method called PROSPECT (primary screening of strains to prioritize expanded chemistry and targets), using a ubiquitin degradation tag, barcoded strains of *Mycobacterium tuberculosis* were screened within a single pool, yielding tenfold more chemical candidates than traditional methods due to the ability to sample a wider range of genetic mutants within a single pool[6]. Meanwhile, the diversity of chemical matter that can be assembled into screening libraries is rapidly expanding. More sophisticated methods to extract and identify biosynthetic gene clusters from soil-dwelling bacteria, which can then be expressed in laboratory strains, are propelling the discovery of natural product antimicrobials[7]. Moreover, screening for natural products in bacteria that share similar requirements for antibiotics as humans, such as those in the gut microbiome of nematodes, led to the discovery of Darobactin, a first-in-class inhibitor of the outer membrane chaperone BamA[8, 9]. While accelerating the discovery of new chemical entities, these modern approaches also exacerbate the critical downstream challenge of mechanism-of-action (MOA) determination to enable candidate development. Currently, extensive biochemical and genetic efforts are required for target and MOA elucidation, which impose major bottlenecks in antibiotic discovery pipelines[5]. More streamlined MOA prediction tools, which ideally can be integrated early into antibiotic development pipelines, are needed to alleviate the bottleneck and guide hit prioritization, medicinal chemistry optimization, and eventual hit-to-lead transition.

Transcriptional profiling of chemical perturbations has long been used to explore the MOAs of antimicrobial agents, first described in yeast using microarray to delineate the MOA of the inhibitor dyclonine [10]. In bacteria, early work in *Bacillus subtilis* generated the first antimicrobial reference set based on gene expression using microarray[11],

98 followed by later work showing conditional mutants underexpressing essential gene targets mimic chemical inhibition
99 of their corresponding gene targets[12]. In the era of next-generation sequencing, genome-wide transcriptomics has
100 replaced microarray as the preferred method to generate affordable gene expression profiling. Over the past decade,
101 gene expression profiling of chemical, environmental or genetic stressors has been performed in a wider array of
102 bacteria, including *B. subtilis*, *M. tuberculosis*, *Staphylococcus aureus*, *Escherichia coli and P. aeruginosa* [11-17].
103 The most extensive expression profiling experiment in *P. aeruginosa* aimed to identify the genetic loci important for
104 antimicrobial resistance[17]. More recently, Espinoza et al. developed a machine learning method for transcriptomics-
105 based MOA prediction in *E. coli*, from which a putative protein synthesis inhibitor was identified based on the similarity
106 of its transcriptional signature compared to the reference set of forty-one antibiotics [15, 18]. This method involves a
107 feature selection algorithm, called *Clairvoyance*, which chooses a set of genes that maximizes its ability to predict the
108 MOA of the known compounds in the reference set.
109
110 Despite the growing affordability and accessibility of genome-wide expression profiling, its broad application in
111 transcriptomics-based MOA prediction remains limited by technical confounding that encumber experimental
112 throughput[19, 20]. Ideally, unbiased transcriptomics-based MOA prediction should be rooted in gene expression
113 responses specific to the given chemical or genetic perturbation. However, during perturbations, bacteria also change
114 the expression of a plethora of background genes, unrelated the perturbed pathway, which obfuscate the
115 perturbation-specific signals. For example, background gene responses relating to growth phase, cellular stress, or
116 late-stage cell death might be shared across a diverse panel of antimicrobial compounds. To minimize confounding,
117 expression profiling experiments require careful, low-throughput experimental designs, in which chemical or genetic
118 perturbations occur in test tubes with close monitoring of the bacterial optical density prior to RNA sampling[11, 12,
119 14, 15]. These experimental approaches, while necessary, are inherently unscalable and impede the expansion of
120 high-quality reference sets into new mechanistic classes or other clinically relevant bacterial pathogens.
121
122 To facilitate the broader applicability of gene expression profiling for MOA prediction, we developed Perturbation-
123 Specific Transcriptional Mapping (PerSpecTM): a reference-based strategy for MOA prediction that leverages its
124 large-throughput scale to accentuate changes in gene expression that are specific to target inhibition or transcriptional
125 repression. We optimized a treatment protocol in which RNA, sufficient in quality and quantify, could be recovered

126 from 60μL of mid-log bacteria under chemical or genetic perturbation in 384-well format. Across this large and diverse
127 population of samples, PerSpecTM leverages z-scoring as the primary metric for relative gene expression to highlight
128 perturbation-specific transcriptional changes, adapted from a strategy previously used in human cancer cell lines[21].
129 We applied PerSpecTM in the important bacterial pathogen *P. aeruginosa*, building two orthologous reference sets:
130 (1) an antimicrobial reference set compressing 37 antimicrobial compounds; and (2) a transcriptional repression
131 reference set comprising 15 strains, each exhibiting tunable transcriptional repression of an essential gene target
132 using CRISPRi. Querying against the antimicrobial reference set, we rapidly elucidated the MOA of three new
133 molecules with anti-pseudomonal activity, and importantly, demonstrated the value of using hypersensitized strains,
134 depleted for essential targets, to yield more robust transcriptional responses to perturbation. Using the transcriptional
135 repression reference set, we then demonstrated proof-of-concept that repressed gene target expression can
136 phenocopy its chemical inhibition, which could afford MOA prediction when no chemical entities exist to serve as a
137 reference. Empowered by PerSpecTM and mutant strains depleted in essential targets, this work enables an
138 unbiased and highly scalable reference-based strategy for MOA elucidation to assist antimicrobial discovery efforts in
139 the face of the looming shortage of antibiotics in healthcare systems worldwide.
140

Results

Developing Perturbation-Specific Transcriptional Mapping (PerSpecTM)

We set out to generate an antimicrobial reference set of chemical treatments of the *P. aeruginosa* laboratory strain UCBPP-PA14 (abbreviated hereafter as PA14) and related mutant strains. We ultimately sought to perform transcriptional profiling in large-throughput format, enabling the generation of hundreds-to-thousands of expression profiles. To enable such scale, we first optimized the assay conditions in 384-well format. Specifically, we determined the optimal cell density, incubation time, and compound concentration for which we could elicit robust transcriptional responses across many different compound treatments.

We first performed an expression profiling time trial on a smaller set of 21 antimicrobial compounds, depicted in bold in **Table 1**, which collectively targeted four distinct cellular mechanisms: DNA synthesis, protein synthesis, peptidoglycan synthesis, and membrane integrity. All expression profiling experiments were performed in 384-well format with 60uL per well at a bacterial inoculum of ~1 x 10^8 CFU/mL (OD_{600} of 0.1). Importantly, for the time trial, antimicrobial agents were dosed at 3-fold their minimum-inhibitory concentrations (MICs) determined by conventional broth microdilution at a much lower inoculum of ~5 x 10^5 CFU/mL[22]. All samples were incubated without shaking for 30, 60, 90, or 120 minutes before chemical lysis, RNA extraction, and RNA sequencing.

The resulting gene expression data were represented as z-scores, calculated for each gene per batch. The z-score provides a measure of gene expression after chemical (or genetic) perturbation relative to the median expression across the entire population of samples within a batch. Provided the batch consists of a diverse set of antimicrobial agents (or genetic perturbations) with multiple MOAs, z-scores highlight transcriptional changes that are unique to a given perturbation, and de-emphasize common gene responses across the population, such as those relating non-specifically to growth, cellular stress, or impending cell death. Thus, the relevant signals are accentuated in an unbiased manner, without needing to optimize or select genes based on *a priori* knowledge. The ability to calculate z-scores across a variety of treatments, rather than just assessing differential expression relative to negative control samples, was made possible by the large-throughput scale of our method. In addition, treatment conditions yielding “transcriptionally weak” responses were removed from the analysis, defined as the differential expression between

168 compound treatment and vehicle treatment wherein no gene had an adjusted p-value that was more significant than
169 the minimum adjusted p-value found when comparing PA14 in water versus DMSO control (i.e. $p_{adj} < 10^{-20}$).
170
171 We then determined the Pearson distances ($\sqrt{(1 - Pearson\ Correlation)}$) of the transcriptional signatures
172 (represented as a z-score value for each gene) between adjacent timepoints over the 120-minute time trial (**Fig. 1a**).
173 The results demonstrated that the transcriptional responses to treatment by inhibitors of DNA synthesis, protein
174 synthesis and membrane integrity plateaued on transcriptional endpoints by 90 minutes. The transcriptional
175 responses to treatment with peptidoglycan synthesis inhibitors were more heterogenous as reflected in their larger
176 Pearson distances, which never fully plateaued even by 120 minutes. We wondered whether the increased
177 transcriptional variability among peptidoglycan synthesis inhibitors related to the inoculum effect, a phenomenon in
178 which antibiotics lose significant activity at high bacterial densities. **Table 1** denotes the antimicrobial compounds
179 exhibiting strong inoculum effects (≥ 4-fold shift in MIC at the high bacterial density) with an asterisk, which comprise
180 all of the peptidoglycan synthesis inhibitors, except imipenem, due to upregulation of the beta lactamase AmpC at
181 high bacterial density[23]. Interestingly, the Pearson distances for imipenem across the time trial also plateau by 90
182 minutes, comparable to inhibitors of protein synthesis, DNA synthesis and membrane integrity. Taken together, these
183 data suggest an incubation time of 90 minutes ensures a stable transcriptional endpoint for most antimicrobial
184 compounds active at the experimental inoculum.
185
186 After establishing an optimal 90-minute intubation time, we sought to determine a general, optimal antimicrobial
187 concentration that elicits a strong transcriptional response. Here we used an expanded set of 39 antimicrobial
188 compounds, shown in **Table 1**, targeting the same four core cellular processes but through more diverse targets. We
189 added several compounds with known anti-pseudomonal activity, but not yet approved for human use. For example,
190 we included cell envelope-related compounds, such as inhibitors of LpxC, LptD, BamA and MreB that disrupt
191 lipopolysaccharide (LPS) biosynthesis, outer membrane protein assembly, and cell shape, respectively. We also
192 included antimicrobial compounds that are not known to act on *P. aeruginosa*, such as the antibiotic nitrofurantoin,
193 which works through a complex mechanism involving reactive oxygen species that interfere non-specifically with
194 protein synthesis, DNA synthesis and cell wall metabolism[24]. We also added: (1) the anti-bacterial agent
195 fosmidomycin, which inhibits Dxr to block isoprenoid synthesis; (2) the Hsp90 inhibitor radicicol, an antifungal agent

196 that likely interferes with gyrase-related proteins with a conserved Bergerat fold[25-27]; (3) the anti-staphylococcal
197 agent fusidic acid, an inhibitor of the elongation factor FusA1 that blocks translation[28]; (4) the antibiotic rifampicin,
198 which blocks transcription through the inhibition of the DNA-dependent RNA polymerase RpoB[29]; (5) the fatty acid
199 synthesis inhibitor thiolactomycin; and (6) the membrane pore former LL-37. Lastly, we included several anti-cancer
200 agents, such as cisplatin, doxorubicin and hydroxyurea, which exhibit antimicrobial activity by inhibiting DNA synthesis
201 through DNA alkylation, deoxyribonucleic acid depletion and DNA intercalation, respectively [30-36].
202
203 In the gene expression dose response experiment, unlike the time trial, all antimicrobial compounds were dosed at an
204 adjusted concentration to account for their MICs at high inoculum (i.e., 1 x 10^8 CFU/mL), thereby correcting for the
205 inoculum effect. Whenever possible, antimicrobial reference compounds were tested at 4-fold, 2-fold and 0.5-fold their
206 MICs determined in broth microdilution experiments at high inoculum. However, by design, not all compounds in the
207 gene expression dose response experiment exhibited anti-pseudomonal activity, allowing us to analyze transcriptional
208 response relative to compound activity. For compounds that were non-lethal, either dosed below their MICs or
209 strongly affected by the inoculum effect, we performed gene expression at their highest possible concentrations based
210 on solubility.
211
212 In general, almost all compounds dosed above their MICs (determined at high inoculum) demonstrated robust
213 transcriptional responses (**Fig. 1b**). In contrast, antimicrobials that were non-lethal yielded variable transcriptional
214 responses. In some cases, such as the DNA synthesis inhibitors and membrane disruptors, robust gene expression
215 signals were generated despite sublethal dosing, suggesting that bacteria are primed to detect non-lethal
216 perturbations of certain cellular processes. In the case of some of the beta lactam antibiotics, such as piperacillin,
217 ceftazidime, and aztreonam, robust transcriptional responses could not be elicited due to compound insolubility at
218 dosing necessary to overcome the inoculum effect (**SI Appendix, Fig. S1**). In fact, aztreonam treatment yielded a
219 transcriptionally weak response across all treatment conditions, and thus it was removed from the reference set
220 construction moving forward. Taken together, these results demonstrate that antimicrobial activity at high
221 experimental inoculum (i.e. 1 x 10^8 CFU/mL) is necessary to ensure a robust transcriptional response to all antibiotics
222 in this large-throughput assay format, even while some compounds are still able to generate robust signals despite
223 sublethal dosing.

224 **Transcriptional responses to antimicrobial compounds with similar MOAs are correlated**

225 As expected, our large-throughput gene expression dataset confirmed that lethal antimicrobial treatments elicited
226 transcriptional responses that correlated by MOA. The Pearson correlations of pairwise combinations of all 90-minute
227 treatments, at the highest dose, are shown as a similarity matrix in **Fig. 1c**. Compounds with limited anti-pseudomonal
228 activity, comprising doxorubicin, radicicol, hydroxyurea, piperacillin, fusidic acid, and rifampicin, had positive
229 correlation values with vehicle treatment. Treatments that were more correlated to vehicle control than any other
230 treatment (including those of the same compound at different doses or time points) were removed from the reference
231 set to ensure that only reliable signals be used for MOA prediction. This requirement removed fusidic acid from the
232 reference set. Of the remaining antimicrobial compounds, Pearson correlations were strongest between compounds
233 sharing the same MOA. Notably, stronger correlations were also observed within antibiotic subclasses. For example,
234 protein synthesis inhibitors separated into subclasses based on the strength of their correlations, grouping together
235 macrolides (clarithromycin and erythromycin), tetracyclines (tetracycline, minocycline and doxycycline) and
236 aminoglycosides (amikacin and gentamicin), while distinguishing them from the other subclasses. Likewise,
237 fluoroquinolones (ciprofloxacin and levofloxacin) formed a clear subgroup within the larger class of DNA synthesis
238 inhibitors. Finally, the transcriptional responses to LptD inhibitors (POL-7001 and POL-7080) and LpxC inhibitors (PF-
239 5081090 and PF-04753299), which block LPS synthesis and transport to the cell surface, respectively, tightly
240 correlated within the group of membrane integrity inhibitors. Meanwhile, despite the resolution obtained for
241 subclasses, the transcriptional responses to inhibitors of membrane integrity and inhibitors of peptidoglycan synthesis
242 also correlated with one another, suggesting a shared cellular response to defects in membrane disruption and
243 peptidoglycan synthesis.

244

245 Lastly, to verify that the transcriptional treatment responses correlated with known biology, we determined the most
246 upregulated and downregulated genes in response to three of the most well-studied antibiotic classes:
247 aminoglycosides, fluoroquinolones and polymyxins. **Table S1** shows the top 25 upregulated and downregulated
248 genes with known annotations in PA14 in response to treatment with aminoglycosides, fluoroquinolone and
249 polymyxins. Indeed, previously reported gene expression signatures were readily apparent for each antibiotic class,
250 providing a cross-check that the PerSpecTM approach indeed highlights changes gene expression directly related to
251 each specific chemical perturbation.

252

253 **Transcriptional responses to treatment of hypersusceptible strains correlate with wildtype treatments**

254 The requirement that compounds have potent wildtype activity to elicit a reliable, robust transcriptional response
255 poses a barrier to the early integration of transcriptomics-based MOA prediction for new compounds found to have
256 some but not highly potent antimicrobial activity. To address this concern, we sought to determine whether
257 hypersusceptible strains could be used in place of wildtype strains to obtain robust transcriptional signals for
258 compounds with limited wildtype activity. While an efflux pump mutant could serve as a hypersusceptible strain in
259 some cases, not all compounds are guaranteed to have increased activity against efflux-deficient strains. We thus
260 selected an alternative strategy that involved engineering hypersensitive mutants by depleting their cognate targets,
261 leveraging the concept of gene dosage in yeast, and later demonstrated in bacteria[6, 37-39].

262

263 We genetically engineered seven hypomorphic strains by depleting the essential gene target corresponding to a set of
264 known antimicrobial agents. Targets with their corresponding on-target antimicrobial included *lptD*-POL7080, *dxr*-
265 fosmidomycin, *murA*-fosfomycin, *gyrA*-ciprofloxacin, *lpxC*-PF-04753299, *dhfR*-trimethoprim, and *bamA*-MRL-494.
266 Most strains were constructed by inserting the target gene at the neutral *attB*-Tn7 site under the control of an artificial
267 promoter (either a constitutive weak promoter or an arabinose-inducible promoter; **Table S2**), followed by deletion of
268 the native gene. In the case of the *lptD* hypomorph, the native promoter was replaced with an arabinose-inducible
269 promoter controlling the entire operon containing *lptD*. The growth phenotypes of most engineered hypomorphs were
270 comparable to wildtype, except for the *gyrA*, *dxr* and *lptD* hypomorphs (**SI Appendix**, **Fig. S2**). We then measured the
271 MICs of compounds for these hypomorphs. The *lptD*, *murA*, and *bamA* hypomorphs were 15 – 20-fold more
272 susceptible to their corresponding gene target inhibitors, POL7080, fosfomycin, and MRL-494, respectively, whereas
273 the *dxr*, *gyrA*, *lpxC* and *dhfR* showed no significant difference from wildtype (**Table S2**).

274

275 We then measured the expression profile of each hypomorph treated with vehicle, one on-target compound (*i.e.,*
276 compound whose activity is due to inhibition of the corresponding target) and two off-target compounds (*i.e.,*
277 compound whose activity is not related to the corresponding target). Hypomorphic strains were incubated with
278 compounds at 2-fold their MICs (determined at high inoculum against each hypomorph), or vehicle, at a final cell
279 density of ~1 x 10^8 CFU/mL for 90 minutes before chemical lysis, RNA extraction, and subsequent library

280 construction. Z-scores were calculated across each hypomorph, rather than across all hypomorphs, to dampen
281 background transcriptional changes related to strain-specific genetic perturbations from the repressed gene target.
282 **Fig. 2** shows a combined uniform manifold approximation and projection (UMAP) showing all 90-minute treatments at
283 the highest dose per strain across the gene expression time trial, dose response and hypomorph experiments. The
284 changes in gene expression of hypomorphs to chemical perturbation correlated with wildtype treatment responses.
285 For example, treatment of the g*yrA*-hypomorph with its on-target inhibitor, ciprofloxacin, grouped with PA14 treatment
286 with ciprofloxacin, as did treatment of the *lpxC*-hypomorph with PF-04753299, *bamA*-hypomorph with MRL-494, *dhfR*-
287 hypomorph with trimethoprim, *murA*-hypomorph with fosfomycin, and *lptD*-hypomorph with POL7080. Meanwhile,
288 using this mutant-specific z-score approach, grouping of mutant and wildtype responses was agnostic of whether a
289 compound's molecular target related to the underlying genetic alteration in a strain, as exemplified by the treatment
290 response of the *gyrA*-hypomorph to doxycycline, a protein synthesis inhibitor unrelated to GyrA, grouping together
291 with PA14 response to doxycycline.
292
293 The correlation between responses of hypersusceptible mutants and wildtype, after adjusting experimental treatment
294 concentrations and computationally accounting for strain-specific transcriptional differences, enables the
295 characterization of expression responses of compounds without wildtype activity. Indeed, the transcriptional response
296 of the engineered *dxr*-hypomorph to fosmidomycin provides proof-of-concept for the utility of using genetically
297 depleted strains to facilitate MOA prediction. Fosmidomycin inhibits Dxr, an essential reductoisomerase in the 2-C-
298 methyl-D-erythritol 4-phosphate (MEP) pathway of isoprenoid precursor biosynthesis [40]. While fosmidomycin
299 exhibited an MIC of 12.5uM at low inoculum, it was inactive against PA14 at the high inoculum used for expression
300 profiling experiments, but delayed growth of the *dxr*-hypomorph (**SI Appendix**, **Fig. S3**). While the expression
301 response of PA14 to fosmidomycin treatment grouped near vehicle controls, the response of the *dxr*-hypomorph
302 grouped with inhibitors of membrane integrity, accurately reflecting the cellular mechanism targeted by fosmidomycin
303 **(Fig. 2).**
304
305 **MOA and target prediction using the antimicrobial reference set**
306 We next set out to evaluate the potential usefulness of the antimicrobial reference set as a tool for predicting the
307 MOAs and targets of novel chemical entities. We first calculated Pearson correlation values between each query and

308 reference treatment, where a treatment refers to a combination of a compound, concentration, time point and strain.
309 After removing any query treatments that are most correlated to vehicle control, the maximal correlation values
310 between the query to each target category are then averaged across all query treatments of the same query
311 compound to produce the final similarity score. Ultimately, the predicted target is determined by the highest overall
312 correlation to the query compound, similar to methods described previously [14]. The predicted MOA of each query
313 compound is then assigned as the known cellular pathway associated with the predicted target.
314
315 To evaluate the performance of this prediction method, we performed a leave-one-out cross validation (**SI Appendix,**
316 **Fig. S4**), wherein the expression profiles for each antimicrobial compound in the reference set were queried against
317 the expression profiles of all other compounds in the reference set. The similarity score analysis predicted correct
318 MOAs for 34 of the 37 antimicrobial compounds (92%), and correct target assignments for 22 of the compounds
319 (60%). Of note, 10 compounds (27%) were the only representatives of their respective target categories, and thus the
320 leave-one-out cross validation had no chance of correct target prediction. Removing those ten singleton compounds
321 from the query, the correct MOA was assigned for 25 out of 27 compounds (94%), and the correct target predicted for
322 22 of the compounds (81%).
323
324 To assess confidence in MOA and target predictions, we next obtained positive predictive values (PPVs) for the
325 prediction of both MOA and target, respectively. The PPV is the percent of compounds in the leave-one-out cross
326 validation whose prediction was correct for a similarity score value above a given threshold. The singleton compounds
327 were included in the calculation of PPV for a more conservative estimate of confidence in target prediction, since they
328 act as proxies for targets not represented by the reference set. Of note, the similarity score distributions are different
329 for different MOAs, and thus may merit different levels of confidence depending on the predicted MOA (**Fig. S4b**).
330 However, due to the limited number of compounds per category, the PPVs were calculated across the entire data set
331 for both MOA and target.
332
333 **External validation of the antimicrobial reference set**
334 We next queried the largest publicly available gene expression dataset in *P. aeruginosa[17]* against our antimicrobial
335 reference set to test whether this MOA prediction approach remained valid despite major differences in experimental

336 design. Indeed, the experimental design of the query gene response dataset was highly divergent from the methods
337 employed in our study. The study aimed to elucidate intrinsic mechanisms controlling antimicrobial resistance, and
338 gene expression experiments comprised duplicate treatments with fourteen antimicrobials (both antibiotics and
339 antiseptics) at sublethal dosing, comprising one fluoroquinolone (ciprofloxacin), three aminoglycosides (gentamicin,
340 neomycin and tobramycin), four peptidoglycan synthesis inhibitors (ampicillin, carbenicillin, cefoperazone and
341 aztreonam), one membrane disruptor (polymyxin B), and five antiseptics (benzalkonium chloride, peroxide, bleach,
342 silver nitrate and povidone-iodine). While the size and chemical diversity of the query dataset allowed us to represent
343 gene expression changes as z-scores, weak transcriptional responses from the sublethal dosing limited the
344 PerSpecTM approach. **Table 2** summarizes the MOA and target predictions of only the chemical treatments having
345 robust transcriptional responses. Of note, the transcriptional response to treatment with tobramycin, ampicillin,
346 carbenicillin, cefoperazone, aztreonam, povidone-iodine, and silver nitrate and were transcriptionally weak, and thus
347 excluded from the analysis. Neomycin also had a transcriptionally weak response but had a meaningful signal and is
348 included in the table. Meanwhile, benzalkonium chloride was most highly correlated to vehicle control and was
349 excluded from analysis.
350
351 Interestingly, the MOA and target were predicted correctly for most of the transcriptionally robust samples (top
352 predictions shown in **Table 2**; full data shown in **SI Appendix**, **Fig. S5**): gentamycin and neomycin were assigned as
353 protein synthesis inhibitors with the 30S ribosomal subunit as the predicted target, and ciprofloxacin was assigned as
354 a DNA synthesis inhibitor with GyrA/ParC as the predicted target. In the case of polymyxin B, the highest similarity
355 score implicated a membrane integrity disruptor with LptD as the potential target, but the similarity score was below
356 that of any compound in the leave-one-out cross validation, and thus could not be assigned a prediction with a known
357 confidence level. Although LptD had the highest similarity score of 0.26, LPS, the known target, was not far behind
358 with a similarity score of 0.23 (**SI Appendix**, **Fig. S5**). Interestingly, of the antiseptics, peroxide was assigned as a
359 DNA synthesis inhibitor with GyrA/ParC as the predicted target, although DNA was not far behind (**SI Appendix**, **Fig.
360 S5**). This finding is supported by the fact that peroxide has been shown to induce oxidative damage and cause
361 double-stranded DNA breaks[41], similar to cisplatin and fluoroquinolones. Meanwhile, bleach was predicted to be a
362 DNA synthesis inhibitor based on highest similarity to nitrofurantoin, a known inducer of ROS production in bacteria.
363 Interestingly, bleach also correlated to many of the inhibitors of membrane integrity, consistent with bleach imparting

364 generalized oxidative damage on both DNA and membranes[42]. These results suggest that external datasets,
365 particularly those of sufficient size and diversity to permit z-score calculations, are amenable to target prediction using
366 the PerSpecTM approach with our antimicrobial reference set.
367
368 Nevertheless, not all external datasets are of sufficient size and diversity to allow z-score calculations. To better
369 validate our antimicrobial reference set using more limited external data, we queried a smaller external dataset[43]
370 against our antimicrobial reference set, which included PA14 treated with DNA inhibitors (ciprofloxacin, levofloxacin,
371 lomefloxacin, novobiocin or DMSO control). Once again, the experimental design of the query dataset diverged highly
372 from our methods: bacteria were exposed to each compound in biological triplicate at sublethal dosing and grown
373 overnight from an optical density of 0.05 to a final density of 0.6 during the exposure. The small size and limited
374 diversity of compound MOAs across this external dataset precluded the use of z-scores across the batch of
375 treatments. Instead, we compared perturbed expressional changes to negative controls by calculating z-scores
376 relative to negative controls, which we termed nz-scores. As summarized in **Table 2** (full data shown in **SI Appendix**,
377 **Fig. S6a**), lomefloxacin was accurately assigned as a DNA synthesis inhibitor with GyrA/ParC as the predicted target
378 based on a similarity score of 0.30 (62% target PPV, 94% MOA PPV). Of note, PPVs for this external dataset were
379 determined by performing the leave-one-out cross validation using nz-scores queried against the z-scores of the
380 reference set. Likewise, novobiocin from this external dataset was assigned as a DNA synthesis inhibitor with GyrB as
381 the predicted target based on a similarity score of 0.26 (58% target PPV, 92% MOA PPV) **(Table 2;** full data shown in
382 **SI Appendix**, **Fig. S6b**). Despite the highly divergent gene expression methodology, these correlation analyses
383 accurately yield accurate MOA and target predictions using our approach. Taken together, these results provide
384 proof-of-concept that external gene expression data can be queried against our reference set to yield helpful
385 mechanistic predictions, and we suspect the confidence of these predictions will grow stronger if care is taken to
386 better reproduce our experimental methods at lethal compound dosing, thereby ensuring robust transcriptional
387 responses from which perturbation-specific gene expression changes can be readily identified with the PerSpecTM
388 method.
389
390
391

392 **MOA and target determination of new screening hits using the antimicrobial reference set**

393 We next sought to test whether PerSpecTM could predict MOAs of new molecules. To this end, we focused on three
394 small molecules we had previously identified using a multiplexed chemical genetic based strategy termed
395 miniPROSPECT[6, 44]. All three compounds were discovered based on their specific activity against certain
396 hypomorphic strains: PA-0918 against *lptD*-hypomorph; PA-69180 against *oprL*-hypomorph; and PA-5750 against
397 *lptE*-hypomorph (**Table 3).** In the case of PA-0918 and PA-5750, we performed expression profiling using PA14
398 because both compounds were active against wildtype. PA-69180 had no wildtype activity, however, and therefore we
399 performed gene expression profiling with the *oprL*-hypomorph, which encodes for the reduced expression of the
400 essential cell wall scaffolding protein OprL.

401

402 PA-0918 was assigned as an inhibitor of membrane integrity with LPS as the predicted target based on a similarity
403 score of 0.74 (100% target PPV, 100% MOA PPV) (**Table 2**; full data shown in **SI Appendix**, **Fig. S7a**). PA-0918
404 most highly correlated with colistin, a polymyxin antibiotic known to target LPS along the outer membrane of Gram-
405 negative bacteria [45-47]. To test whether PA-0918 shares a similar mechanism-of-action with colistin as a direct
406 membrane disruptor, we utilized an ethidium bromide uptake assay, in which membrane disruption is detected by
407 increased flux of ethidium bromide into the cells. We found that PA-0918 phenocopies colistin's ability to promote
408 rapid uptake of ethidium bromide into cells (**SI Appendix**, **Fig. 8**), consistent with PA-0918 disrupting the outer
409 membrane to increase permeability.

410

411 Using the *oprL*-hypomorph, PA-69180 was predicted as a peptidoglycan synthesis inhibitor with MreB, the major Rod
412 protein responsible for the rod shape of gram-negative bacteria, as the predicted target based on a similarity score of
413 0.38 (68% target PPV, 94% MOA PPV) (**Table 2**; full data shown in **SI Appendix**, **Fig. S7b**). To test whether PA-
414 69180 could be an MreB inhibitor, we used a mecillinam rescue assay described previously [48], which leverages the
415 fact that overexpression of the cell-division protein FtsZ in *E. coli* (strain MG1655/FtsZup) renders the Rod system
416 non-essential, thus conferring resistance to MreB inhibition. Meanwhile, MreB inhibition in this strain reverses the
417 lethal effects of the penicillin binding protein 2 inhibitor mecillinam, which otherwise causes a toxic malfunctioning of
418 the Rod machinery leading to cell death. We found that PA-69180 phenocopies the known MreB inhibitor A22, with
419 MG1655/FtsZup being both resistant to PA-69180 killing and resistant to mecillinam killing upon the addition of PA-

420 69180 (**Table S3**). We also generated resistant mutants to PA-69180 in the efflux-deficient strain PAO397 and
421 performed whole-genome sequencing to reveal single nucleotide polymorphisms (SNPs) driving point mutations in
422 MreB that conferred resistance (**Table S4**). Two mutants, PAO397-r1 and PAO397-r3, had mutations at distinct amino
423 acid positions adjacent to the ATP binding pocket of MreB that conferred high-level resistance to PA-69180 and
424 cross-resistance to A22 based on 32–64-fold shifts in MIC relative to the parent PAO397 strain, thereby confirming
425 MreB as the target (**Table S5**).
426
427 Finally, PA-5750 was assigned as a DNA synthesis inhibitor with GyrA/ParC as the predicted target based on a
428 similarity score of 0.56 (88% target PPV, 96% MOA PPV) (**Table 2**; full data shown in **SI Appendix**, **Fig. S7c**). Based
429 on this prediction, we immediately moved to testing PA-5750's ability to both intercalate DNA or inhibit DNA gyrase.
430 To probe for DNA intercalation, we utilized the human topoisomerase I DNA unwinding assay, which identifies
431 molecules that intercalate relaxed DNA, thereby altering the linking number to stimulate supercoiling activity of
432 topoisomerase I. There was no evidence of DNA intercalation by PA-5750, or the negative control ciprofloxacin,
433 based on the absence of supercoiled DNA, in contrast to the known DNA intercalator m-amsacrine (m-AMSA) (**SI**
434 **Appendix**, **Fig. S9a**). In a complementary assay, in which DNA intercalators displace ethidium bromide from purified
435 plasmid, we showed that m-AMSA exhibited a dose-dependent displacement of ethidium bromide from purified
436 plasmid, whereas PA-5750 and ciprofloxacin did not substantially displace ethidium bromide (**SI Appendix**, **Fig. S9b**).
437 Having ruled out PA-5750 as a DNA intercalator, we next tested whether PA-5750 inhibited *E. coli* DNA gyrase's
438 ability to supercoil DNA. Indeed, we found that PA-5750 reduced the amount of supercoiled plasmid generated by
439 DNA gyrase in a manner similar to known gyrase inhibitors ciprofloxacin and novobiocin (**SI Appendix**, **Fig. S9c**),
440 while the R enantiomer of PA-5750, which has no antibacterial activity, showed no gyrase inhibition. Lastly, based on
441 the observation that gyrase overexpression leads to ciprofloxacin hypersusceptibility through increased double-
442 stranded DNA breaks[49], we sought to test the impact of gyrase overexpression on PA-5750 activity. We engineered
443 a PAO1 strain that overexpressed both *gyrA* and *gyrB* episomally under the control of rhamnose. Indeed,
444 overexpression of gyrase led to an increase in susceptibility to PA-5750 (**SI Appendix**, **Fig. S9d**). Taken together,
445 these results support the prediction of PA-5750 as targeting gyrase, and overall, validate the ability of this expression-
446 based approach to MOA predictions.
447

448 **Assessing the transcriptional signatures of hypomorphic strains**

449 With the well-validated reference set in hand, we sought to test whether the transcriptional signals of hypomorphic
450 strains correlate with chemical inhibition of their gene products. This is an important question to ascertain because our
451 transcriptomics-based MOA prediction strategy relies on a reference set built exclusively of compounds that
452 chemically inhibit gene products in essential cellular pathways. However, there are other attractive gene targets
453 without known inhibitors, which would show up as “blind spots” in MOA prediction analyses. If the transcriptional
454 repression of a gene product phenocopies its chemical inhibition, then using the transcriptional responses of
455 hypomorphic strains could be a powerful approach for predicting the transcriptional profile of gene targets without
456 known inhibitors. If feasible, a comprehensive set of hypomorphic strains could in theory provide the blueprint for
457 every targetable pathway, facilitating a more complete reference set for MOA prediction of screening hits.

458

459 To this end, we reanalyzed the hypomorph gene expression data to investigate whether background transcriptional
460 response in hypomorphic strains phenocopied wildtype treatment with on-target control compound. In this new
461 analysis, z-score calculations were instead carried out across all genetic mutants, rather than within each strain, to
462 include strain-specific transcriptional differences in our analyses. Pearson correlations were stronger between genetic
463 mutants and untreated PA14 rather than between the genetic mutants and PA14 treated with on-target control
464 compounds (**SI Appendix**, **Fig. S10**), indicating that transcriptional signatures of hypomorphic strains could not
465 reliably predict the transcriptional profile of chemical inhibition of the target gene of interest.

466

467 **Assessing the transcriptional signatures of CRISPRi strains**

468 We wondered whether the transcriptional responses of genetic hypomorphs were dampened due to the lack of acute
469 perturbation in these systems. When hypomorphic strains were controlled by weakened promoters, we postulated that
470 transcriptional changes might to dissipate over time as cells adapt gradually to restrictive gene expression. We
471 therefore shifted to a genetic system designed to induce gene repression more rapidly to better mimic the effect of
472 chemical inhibition by small molecules. We specifically turned to CRISPRi technology to create an inducible gene
473 repression system, in which arabinose could be added to downregulate gene expression at the transcriptional level in
474 a dose-dependent manner. This new approach would allow stable cell growth in the absence of arabinose, followed
475 by more sudden perturbation through the transcriptional repression of target genes by arabinose exposure at the very

476 beginning of the gene expression experiments. We constructed eighteen CRISPRi strains encoding arabinose-
477 induced dCas9 at the neutral *attB*-Tn7 site alongside constitutively expressing guide RNAs targeting no gene (so-
478 called CRISPRi-*C26*), *dhfR*, *dxr*, *gyrA*, *gyrB*, *leuS*, *lptA*, *lptD*, *lptE*, *lpxC*, *mreB*, *murA*, *parC*, *pbpA*, *ssb*, *rplJ*, *rpoB* and
479 *rpsL*, summarized in **Table S6**. In each CRISPRi strain, the addition of arabinose drove dCas9 expression and
480 subsequent transcriptional repression of the target gene of interest. We characterized the arabinose-dependent
481 growth phenotypes of each CRISPRi strain (**SI Appendix**, **Fig. S11**). The CRISPRi-C26 control strain showed no
482 significant growth delay over an arabinose range of 0 – 0.5% (w/v), indicating no appreciable dCas9-mediated toxicity
483 in PA14. CRISPRi-*dhfR*, CRISPRi-*lptA*, CRISPRi-*lpxC*, CRISPRi-*mreB*, CRISPRi-*murA* and CRISPRi-*parC* all
484 demonstrated severe arabinose dose-dependent growth delays, whereas CRISPRi-*dxr*, CRISPRi-*gyrA*, CRISPRi-
485 *gyrA-2,* CRISPRi-*gyrB*, CRISPRi-*leuS*, CRISPRi-*lptD*, CRISPRi-*lptE*, CRISPRi-*rplJ*, CRISPRi-*rpoB* and CRISPRi-*rpsL*
486 exhibited more moderate growth delays at higher arabinose concentrations. By comparison, CRISPRi-*pbpA* and
487 CRISPRi-*ssb* showed no significant growth delay.
488
489 We next performed high-throughput gene expression profiling of all CRISPRi strains at 360 minutes in 0%, 0.125%,
490 and 0.5% arabinose before chemical lysis, RNA extraction, and subsequent library construction. Z-scores were
491 calculated across all strains and arabinose doses, thereby accentuating strain-specific transcriptional changes. As
492 summarized in **Table S7**, CRISPRi strains in general demonstrated an arabinose-dependent decrease in target
493 mRNA levels at 360 minutes compared to the CRISPRi-*C26* control strain, ranging from 1.5 – 174-fold in 0.125% or
494 0.5% (w/v) arabinose for conditions yielding p-values below 0.05. Notably, gene expression changes were not
495 statistically significant across both arabinose conditions (i.e. 0.5% and 0.125%) for CRISPRi-*lptE*, and CRISPRi-*ssb*
496 and CRISPRi-*rpoB*.
497
498 Next, we assessed whether the transcriptional profiles of the CRISPRi strains could potentially serve as a reference
499 set from which we could predict targets of unknown compounds. We utilized the same MOA prediction method as in
500 the previous sections, using z-scores of the CRISPRi strains as the reference set (across both doses of arabinose
501 above 0% at 360 minutes), and queried the transcriptional responses of 90-minute antibiotic treatments, comprising
502 an on-target agent for each CRISPRi strain. All compound treatments were against wildtype PA14, except for
503 fosmidomycin, which was used against the *dxr*-hypomorph strain since it was not active against PA14. We again

504 removed treatment conditions yielding “transcriptionally weak” responses, defined as the differential expression
505 between arabinose treatment and control guide C26 wherein no gene had an adjusted p-value that was more
506 significant than the minimum adjusted p-value of PA14 in water versus DMSO control (i.e. $p_{adj} < 10^{-20}$). Applying this
507 filter, CRISPRi-*dhfR*, CRISPRi-*gyrA-2*, CRISPRi-*leuS*, and CRISPRi-*lptE* were removed from analysis on account of
508 their weak transcriptional responses.
509
510 As shown in **Fig. 3**, the transcriptional responses of antibiotic treatments generally correlated to transcriptional
511 responses of their associated CRISPRi strains. These results demonstrate accurate target predictions in many cases.
512 For example, ciprofloxacin treatment correlated strongest with CRISPRi-*parC,* followed by CRISPRi-*gyrA*, accurately
513 mapping to its known target of GyrA/ParC. Similarly, the GyrB inhibitor novobiocin correlated strongest to CRISPRi-
514 *gyrB*; the LpxC inhibitor PF-04753299 mapped to CRISPRi-*lpxC*, the LPS transport inhibitor POL7080 mapped to
515 CRISPRi-*lptA*, the MurA inhibitor mapped to CRISPRi-*murA*, and the aminoglycoside amikacin mapped to CRISPRi-
516 *rpsL*. In cases of incorrect target prediction, the MOAs of the query compounds were still accurately predicted for all
517 but two of the compounds. For example, all protein synthesis inhibitors (amikacin, clarithromycin, and rifampicin)
518 correlated strongest with the three CRISPRi strains designed to interfere with protein synthesis, CRISPRi-*rpsL*,
519 CRISPRi-*rplJ* and CRISPRi-*rpoB*. Similarly, fosmidomycin was correctly predicted to disrupt membrane integrity. Of
520 the two compounds with misassigned MOAs, the peptidoglycan synthesis inhibitors A22 and imipenem, both were
521 predicted to be membrane disruptors and still correlated to a lesser extent to CRISPRi strains disrupting
522 peptidoglycan synthesis. Moreover, inhibitors of membrane integrity and peptidoglycan synthesis tended to correlate
523 across mechanistic classes in general, suggesting a shared transcriptional response to disruption of in either cellular
524 process. We wonder whether this observation may relate to the recent discovery that MurA stimulates LpxC through
525 direct biochemical interaction[50], linking the regulation of peptidoglycan biosynthesis with that of membrane integrity.
526 Taken together, these data demonstrate that the transcriptional response of chemical inhibition of a given gene target
527 correlates with CRISPRi-induced repression in gene expression, providing proof-of-concept that CRISPRi strains
528 could be integrated in chemical screening pipelines to facilitate MOA prediction of gene targets without available
529 chemical inhibitors.
530
531

532 **Discussion**

533 Target identification is central to any antibiotic discovery pipeline by building confidence in hits and guiding medicinal
534 chemistry efforts towards chemical optimization. The advancement of more sophisticated approaches to antibiotic
535 discovery has greatly expanded the chemical screening space and increased the number of primary hits discovered
536 from target-based screens in whole cells. While exciting, these novel platforms further exacerbate the bottleneck that
537 target identification already imposes on antibiotic development efforts. Moreover, the risk of rediscovering similar
538 compounds across screens, particularly those hindered by toxicities or resistance vulnerabilities, could be mitigated
539 by integrating MOA prediction tools earlier in screening pipelines to better prioritize hits.

540

541 Transcriptional-based approaches for target identification are particularly beneficial because they concurrently yield
542 valuable insights into the biology of how target disruption leads to killing. Other groups have long-established
543 expression profiling as a valuable tool for MOA prediction in bacterial pathogens[11-16]. To date, however,
544 background changes in gene expression – those relating to growth, general stress, or cell death – drown out
545 perturbation-specific gene responses, necessitating experimental designs that control for background gene
546 expression and limit the throughput and broad applicability of this approach. The novelty of PerSpecTM lies in its
547 scale: low sample volumes in 384-well format afford an unprecedented diversity of chemical or transcriptional
548 perturbations within a single experimental batch. Paired with the calculation of z-scores across this diverse sample
549 set, PerSpecTM highlights perturbation-specific changes in gene expression that drive accurate MOA prediction
550 without the need for complex methods or *a priori* knowledge to select subsets of genes, or rigorous experimental
551 control of non-specific changes in background gene expression. Importantly, antimicrobial activity was necessary to
552 ensure a robust transcriptional response to chemical treatments, which poses a barrier for MOA prediction of new
553 compounds that lack wildtype activity. While an efflux pump mutant could serve as a hypersusceptible strain for some
554 compounds, not all compounds exhibit increased activity in such strains. Thus, we engineered hypomorphic strains
555 that are hypersensitized to inhibitors by depleting their cognate targets. Importantly, for compounds lacking wildtype
556 activity, we showed that hypomorphic strains could be incorporated into PerSpecTM to facilitate MOA prediction
557 because antimicrobial compounds grouped by MOA agnostic of genetic strain. We subsequently validated our
558 antimicrobial reference set with accurate MOA prediction of both internal and external datasets.

559

560 Our three internal screening hits – PA-0918, PA-69180 and PA-5750 – highlight the power of MOA determination
561 early in the antibiotic discovery process. All three compounds originated directly from chemical libraries, and therefore
562 had not yet undergone extensive structure-activity-relationship studies. We rapidly identified PA-0918 as a membrane
563 disruptor, PA-69180 as an MreB inhibitor, and PA-5750 as an inhibitor of DNA gyrase. The case of PA-69180, which
564 lacked significant wildtype activity, highlights the advantage of leveraging the *oprL*-hypomorph to generate a robust
565 transcriptional signal. The case of PA-5750, which was discovered based on its activity against the *lptE*-hypomorph,
566 adeptly highlights the advantage of integrating MOA prediction tools early in the discovery process. Based on its
567 activity against the *lptE*-hypomorph, which has a deficit in the LPS transport system, we expected PA-5750 to act on a
568 cellular pathway relating to LPS biosynthesis, transport, or membrane biology in general. However, based on the
569 results of PerSpecTM, we instead identified PA-5750 as a gyrase inhibitor, which ultimately guided us away from
570 efforts towards chemical optimization at such an early stage after its discovery. Early target elucidation of PA-5750
571 also demonstrates how PerSpecTM can help address the major liability that antimicrobial activity against hypomorphs
572 might relate to changes in membrane integrity that enhance xenobiotic uptake, rather than directly to the repressed
573 gene target. Taken together, these data support the earlier integration of genome-scale transcriptional profiling in
574 antibiotic discovery pipelines to facilitate MOA prediction of chemical screening hits, which can help guide hit
575 prioritization ahead of chemical optimization and eventual the hit-to-lead transition.
576
577 Referenced-based MOA prediction by expression profiling is inherently limited by the diversity of the reference set,
578 which poses a barrier to discovering inhibitors of novel genetic pathways without known chemical inhibitors. We
579 therefore explored an orthologous approach by constructing a transcriptionally repressed reference set using
580 CRISPRi technology. We demonstrated that chemical inhibition of a series of gene targets correlated strongest with
581 their corresponding CRISPRi knockdown strains. Importantly, our results suggest that the least fit CRISPRi strains,
582 such as CRISPRi-*parC*, CRISPRi-*lptA*, yielded the strongest Pearson correlations to chemical inhibition of their
583 corresponding gene targets. Thus, any CRISPRi-based MOA prediction approach will rely on the fitness level across
584 the CRISPRi strains in the reference set. In our case, we constructed a small set of CRISPRi strains without
585 significant focus on the fitness level of each strain. In future iterations of this approach, we believe first employing a
586 chemical-genetic platform to quantify bacterial fitness of a larger library of CRISPRi strains, as reported previously in
587 *M. tuberculosis*[51], would yield a stronger CRISPRi reference set and generate more robust correlations for MOA

588 predictions. Nevertheless, these data provide proof-of-concept that a dedicated CRISPRi reference set could facilitate
589 accurate MOA prediction, including for gene targets without known chemical inhibitors. In theory, a library of CRISPRi
590 strains could be used to define the transcriptional map of all essential genes of a certain bacterium, serving as a
591 reference set for screening hits with unelucidated targets, or new targets without known small molecule inhibitors.
592
593 Despite the upside to transcriptomic-based MOA prediction platforms, certain downsides warrant consideration. First
594 and foremost, a significant amount of time, effort and funding is necessary to build a reference set for a given bacterial
595 pathogen. While we show the reference set for *P. aeruginosa* is useful for MOA prediction in other pseudomonas
596 strains, new reference sets will need to be built from the ground up for MOA prediction platforms in other important
597 bacteria, such as *Klebsiella pneumoniae*, *Acinetobacter baumannii*, and other high-priority Gram-negative bacterial
598 pathogens. Moreover, transcriptional sequencing still requires a level of knowledge, experience and access that
599 prevents data sharing across groups of scientists. In addition, transcriptional profiling at scale in 384-well format adds
600 further cost to an already expensive endeavor, especially because PerSpecTM requires a diverse set of samples
601 within any plate for z-scores to highlight perturbation-specific changes in gene expression. At a minimum, this would
602 require a query compound to be tested along with vehicle control and at least three other compounds, each one
603 representing a different MOA (DNA synthesis, Protein Synthesis, and either Peptidoglycan Synthesis or Membrane
604 Integrity), as we demonstrated with the hypomorph data. For data sets with low diversity in represented MOAs, we
605 employed nz-scores to validate our chemical reference set against external data, which requires only vehicle control
606 as the comparator. Though not as robust as z-scores, we think this approach will make our data more accessible to
607 other groups, who could use nz-scores and query unknown compounds, alongside a vehicle control, if they are unable
608 to include additional diverse antibiotics. By sharing our PerSpecTM approach, and associated reference sets, we
609 hope to lower this barrier by allowing other groups to integrate their own gene expression data into our pipeline.
610
611 Lastly, while gene expression profiling relies on transcriptional responses across a reference set of chemical
612 perturbations, other genomic-based strategies are equally valid as MOA prediction that also provide insights into
613 chemical-genetic interactions. Strategies aimed at modulating gene target expression can impact the sensitivity to
614 small molecule inhibitors, as overexpressed and underexpressed targets will decrease and increase sensitivity,
615 respectively [39, 49]. Indeed, transposon libraries were used to combine overexpression and underexpression

616 approaches in a single system, in which an outward-facing promoter within the transposon drove, suppressed or
617 abrogated gene expression [52]. In an approach called phenomic profiling, gene deletion libraries or transposon
618 libraries have been deployed to facilitate MOA prediction by mapping gene interactions in response to chemical
619 treatments, allowing for network mapping predicting MOA [17, 53, 54]. As we look to the future, CRISPRi libraries
620 could be used to generate the transcriptional responses to knockdown any essential gene product, even those without
621 a known chemical inhibitor, thereby creating a more expansive transcriptional landscape that could serve as a
622 reference for future antibiotic discovery initiatives.
623

Materials and Methods

Bacterial strain construction

All *P. aeruginosa* strains used for gene expression experiments were derived from the UCBPP-PA14 lab strain as described previously[55]. The DNA gyrase overexpression strain was derived from PAO1[56]. **Table S8**, **Table S9** and **Table S10** describe all plasmids, strains and primers used in this study. Detailed methods describing all strain construction are available in the **Additional Methods** of **SI Appendix**.

MIC determination and growth kinetics

All MIC and growth kinetic experiments were conducted in biological triplicate in 384-well microplates (Thermo Fisher Scientific, Waltham MA) using the broth microdilution method previously described[22]. All arabinose-inducible hypomorphic strains were grown initially in the presence of 0.25% (v/v) arabinose in LB, and subsequently sub-cultured without arabinose. Growth curves of hypomorphic strains were performed without arabinose by back-diluting mid-log cultures to $5x10^5$ CFU/mL bacteria (OD_{600} 1.0 = 10^9 CFU/mL based on plate counts). Growth curves for all CRISPRi strains were performed at various doses of arabinose, the inducer of dCas9. For MIC assays at high inoculum, mid-log bacterial cultures were diluted to 1 x 10^8 CFU/mL bacteria (OD_{600} 1.0 = 10^9 CFU/mL based on plate counts). Antimicrobial compounds were serially diluted in either DMSO or water to a final concentration of 0.5% (v/v). For MIC experiments, microplates were incubated in a humidity chamber without shaking for 16 hours at 37°C, after which time the OD_{600} was measured in the Spark Multimode Reader (Tecan, Männedorf Switzerland). For growth kinetics, Microplates were incubated in a large humidity cassette in the Spark Multimode Reader (Tecan, Männedorf Switzerland) for 24 hours at 37°C, and OD_{600} measurements were recorded after 30-seconds of shaking every hour. Data were plotted and analyzed using GraphPad Prism10 (GraphPad Software, Boston MA) to determine growth kinetic curves or MICs, the latter defined as the minimal compound concentrations required for complete inhibition of bacterial growth.

Gene expression experiments, sequencing, and analysis

Gene expression experiments were carried out in biological triplicate in 384-well microplates (Thermo Fisher Scientific, Waltham MA). Bacterial cultures were grown in LB with shaking (37°C, 250rpm) to mid-log phase. Meanwhile, stock solutions of compounds were dissolved fresh in DMSO or water, and 30μL of compound solutions

652 were mixed with 30μL of mid-log culture to yield $1x10^8$ CFU/mL bacteria and compounds in 0.5% (v/v) DMSO or water
653 in LB. Cells were treated at 37°C without shaking in a humidity chamber. In the case of the gene expression time
654 trial, cells were treated for 30, 60, 90, and 120 minutes. In the case of the CRISPRi strains, cells were treated for 360
655 minutes. In all other experiments, cells were treated for 90 minutes. At the end of the incubation period, samples were
656 then mixed with 30μL of 3X RNAgem Blue Buffer (Zygem, Charlottesville VA), chemically lysed by incubation in a
657 thermocycler at 75°C for 10 minutes, flash frozen and stored at -80°C.
658

659 **Generation of gene expression libraries**

660 Total RNA was extracted using the Direct-zol kit (Zymo Research, Irvin CA), and RNA quality and quantity were
661 analyzed using the RNA ScreenTape with the 2200 TapeStation (Agilent, Santa Clara CA). Illumina cDNA libraries
662 were generated using a modified version of the RNAtag-seq protocol[57]. Briefly, 250ng of extracted RNA was
663 fragmented, dephosphorylated, and ligated to DNA adapters carrying 5'-AN_8-3' barcodes of known sequence with a 5'
664 phosphate and a 3' blocking group. Barcoded RNAs were pooled and depleted of rRNA using the Pan-Bacteria
665 riboPOOL depletion kit (siTOOLs Biotech, Galen Laboratories). Pools of barcoded RNAs were converted to Illumina
666 cDNA libraries in 2 main steps: (i) reverse transcription of the RNA using a primer designed to the constant region of
667 the barcoded adaptor with addition of an adapter to the 3' end of the cDNA by template switching using SMARTScribe
668 (Clontech) as described[58]; (ii) PCR amplification using primers whose 5' ends target the constant regions of the 3' or
669 5' adaptors and whose 3' ends contain the full Illumina P5 or P7 sequences. cDNA libraries were sequenced on the
670 Illumina [NovaSeq SP 100] platform to generate paired end reads.
671

672 **Computational analysis of gene expression profiling**

673 *Processing raw reads*

674 Sequencing reads from each sample in a pool were demultiplexed based on their associated barcode sequence using
675 custom scripts, allowing up to 1 mismatch in the barcode. Barcode sequences were removed from the first read as
676 were terminal G's from the second read that may have been added by SMARTScribe during template
677 switching. Sequencing reads were aligned to the UCBPP-PA14 (NC_0088463.1) reference sequence using BWA[59],
678 assigned genomic features using custom scripts, and visualized using GenomeView[60]. Samples that had low read

679 counts, where over 80% of the genes had zero counts, were filtered out of the data set. In addition, any genes that
680 had zero counts in 50% or more of the samples in a sequencing batch were removed.
681
682 *Assessing robustness of transcriptional response*
683 To assess the level of differential gene expression induced by each treatment condition, DESeq2[61] was used to
684 calculate the $\log_2$ fold change and adjusted p-values (with target false discovery rate, or FDR, set to 0.05) for each
685 gene relative to control. However, even small changes to the environment can lead to changes in gene expression
686 that may reach statistical significance, although not biologically interesting. We used the comparison of PA14 gene
687 expression between DMSO and water as a baseline for setting a threshold to separate "weak" from "robust"
688 responses. Specifically, for a treatment condition to be considered as having a robust transcriptional response, we
689 require that at least one gene be different from the negative control with an adjusted p-value that is smaller than 10^{-20}.
690 Such robust conditions were included in the reference set, while weak ones were excluded. Although some weaker
691 signals may reflect meaningful biological changes, we wanted to only include robust signals in the reference set to
692 predict mechanisms of unknown compounds more reliably. To further ensure that only reliable transcriptional
693 signatures were used to predict MOA, we additionally removed any treatment conditions whose transcriptional
694 response correlated more highly to negative control conditions than any other condition in the data set, including other
695 time points or doses of the same compound.
696
697 *Calculation of moderated z-scores and nz-scores*
698 Read counts were transformed using the variance stabilizing transformation from the DESeq2 package (v1.28.1) in R
699 (4.0.0)[61]. Then, to identify gene expression changes of interest, moderated z-scores were calculated as described
700 previously[21]. More specifically, robust z-scores (using medians and median absolute deviations) for each gene were
701 calculated per batch, where each batch is defined as all the treatments on the same 384-well plate that share a strain
702 and time point. In cases where there was not a diverse set of mechanisms represented by the compounds in the
703 batch, expression levels were standardized using the median and median absolute deviations of only the negative
704 control samples from each batch, rather than all the treatments in the batch. We termed these values "nz-scores" (z-
705 scores relative to negative controls). The data sets that used nz-scores in this manuscript were the external data set
706 of DNA synthesis inhibitors [43] and the screening hit PA-69180 that was used to treat the oprL-hypomorph. All other

707 data involved a diverse set of compounds within each batch, such that z-scores could be calculated. Next, replicate
708 data were combined using a weighted average, where the weights were determined by the Spearman correlation
709 between replicate transcriptional profiles, as described previously[21]. Finally, extreme z-score values were clipped
710 such that fewer than 1% of the values were affected. For the reference set, z-score values lower than -10 were set to -
711 10, and those higher than 10 were set to 10, so that extreme values would not spuriously impact downstream
712 correlation values. After calculation of all z-score values, transcriptional data were visualized using a UMAP[62],
713 implemented by the R package umap (v0.2.10.0).
714
715 *Selection of marker genes to validate transcriptional responses with known biology*
716 Within each antibiotic class, the z-score gene responses to 90-minute compound treatment were sorted for strength
717 (i.e. absolute value of z-score) and consistency (i.e. same sign of z-score across all samples). If the z-scores for a
718 given gene had disparate signs within the antibiotic class, that gene was removed from analysis for that class. Top up-
719 and down-regulated genes were assessed for validation with known biology of the targets.
720
721 *Prediction of compound targets and leave-one-out cross validation*
722 The reference set of transcriptional profiles was used to predict the targets of unknown compounds by using Pearson
723 correlation values. Depending on the composition of each query data set, z-score or nz-scores were calculated.
724 Individual query compound treatments (e.g. multiple doses or time points) were correlated to the reference set z-score
725 values. A similarity score was then generated between the query compound and each target category using all
726 available treatments of the query compound, and all available treatments of the target category in the reference set.
727 For each query treatment, the maximal Pearson correlation to all the treatments in the given target category was
728 recorded. Any query treatment that was most highly correlated to vehicle control was removed. Then, if there were
729 multiple remaining treatments for the given query compound, the average of their recorded maximal correlation values
730 was calculated to be the similarity score for each target category. The target category with the highest similarity score
731 then was taken to be the predicted target of the query compound, similar to the method described previously[8]. Each
732 target category is a component of a more general MOA category, so the MOA prediction for the query compound
733 follows directly from target prediction.
734

735 The leave-one-out cross validation of the method was performed in the manner described above, wherein each
736 compound in the reference set was taken to be a query compound. When querying a given compound, all other
737 instances of the same compound (e.g. different doses, time points, or strains) were removed from the reference set.
738 Target predictions were made for each compound, and corresponding MOA predictions were assigned. Furthermore,
739 the positive predictive values (PPVs), i.e. the percent of compound targets predicted correctly at each similarity score
740 threshold, were recorded during the leave-one-out cross validation to be used as a measure of confidence for
741 predictions on unknown compounds. Note that target categories comprised of only one compound (27% of
742 compounds), which could never be predicted correctly in the leave-one-out cross validation, were maintained in the
743 calculation of PPV to obtain a conservative estimate. PPV was calculated both at the level of specific target prediction,
744 and at the level of general MOA prediction. Also, the leave-one-out cross validation was performed for querying both
745 z-scores and nz-scores, separately, so that PPVs could be assigned for queries using z-scores and nz-scores
746 appropriately. PPVs were calculated using the pROC library (v1.16.2) in R. Predictions with similarity scores below
747 the minimum similarity score in the leave-one-out cross validations were assigned a PPV of NA, since no confidence
748 could be assessed due to being out of the range of our reference data.
749
750 *Assessing transcriptional similarity of hypomorphic strains to wildtype treated with matched compounds*
751 To assess the similarity of transcriptional profiles of hypomorphic strains to those of wildtype treated with a matched
752 compound, the definition of the batch was further restricted to treatments on the same 384-well plate sharing a time
753 point, thereby allowing different strains to be included in the same batch and revealing strain-specific transcriptional
754 signals. Pearson correlation values were then calculated between these z-scores and those from wildtype treated with
755 a compound targeting the same gene, as well as to those from wildtype with vehicle, all from the same 384-well plate.
756
757 *Using transcriptional profiles of CRISPRi strains to predict compound mechanisms*
758 Transcriptional data from the CRISPRi strains were processed in the same manner as those from compound
759 treatments. Z-scores were calculated for each gene across all CRISPRi samples at all doses of arabinose. Differential
760 gene expression between each sample and the control strain (CRISPRi-C26) at matched doses of arabinose was
761 used to assess the strength of transcriptional response. The same p-value threshold as before was used to filter out
762 weak signals. Then, predictions of compound mechanism and target were performed in the same manner as

763 described earlier, except using the CRISPRi transcriptional profiles as the reference data set. Pearson correlation
764 values were calculated between the z-scores of the CRISPRi strains and those of the wildtype strain treated with
765 different compounds targeting the same genes as the CRISPRi constructs. The exception was fosmidomycin where
766 the *dxr*-hypomorph strain was used instead of wildtype since the compound was not active against wildtype PA14. A
767 similarity score between transcriptional profiles of each compound (query) and each CRISPRi strain (reference set)
768 was calculated in the same manner as described above. The transcriptional data used as the query were the relevant
769 90 minute treatments from the antimicrobial reference data set.
770
771 *Scripts and data accessibility*
772 Scripts for calculating z-scores, nz-scores and predicting compound targets were written in R and stored in github
773 (https://github.com/broadinstitute/psa_rnaseq_manuscript_rproject). Other researchers may utilize the reference data
774 set to predict targets or affected cellular mechanisms using transcriptional data from compounds with unknown
775 mechanisms. All raw sequencing data and z-score values can be found on the Gene Expression Omibus (GEO
776 accession GSE251671, https://www.ncbi.nlm.nih.gov/geo/)
777
778 **Biochemical characterization of screening hits**
779 Resistance selection experiments, as well as assays quantifying ethidium bromide uptake and displacement,
780 mecillinam rescue, DNA intercalation, and DNA gyrase activity, are described in detail in the **Additional Methods** of
781 the **SI Appendix**.
782

Acknowledgments

This work was supported by a generous gift from Anita and Josh Bekenstein and NIH grant 1R01AI117043-04 (D.T.H). Gene expression libraries were constructed and sequenced at the Broad Institute of MIT and Harvard by the Microbial 'Omics Core and Genomics Platform, respectively. The Microbial 'Omics Core also provided guidance on experimental design and conducted preliminary analysis for all gene expression data. We thank Nirmalya Bandyopadhyay, James Gomez, and Roby Bhattacharyya for their helpful discussions. We declare that we have no conflicts of interest. All figures were created with BioRender.com.

References

1. Magill, S.S., et al., *Multistate point-prevalence survey of health care-associated infections.* N Engl J Med, 2014. **370**(13): p. 1198-208.
2. Willyard, C., *The drug-resistant bacteria that pose the greatest health threats.* Nature, 2017. **543**(7643): p. 15.
3. Breidenstein, E.B., C. de la Fuente-Nunez, and R.E. Hancock, *Pseudomonas aeruginosa: all roads lead to resistance.* Trends Microbiol, 2011. **19**(8): p. 419-26.
4. Lister, P.D., D.J. Wolter, and N.D. Hanson, *Antibacterial-resistant Pseudomonas aeruginosa: clinical impact and complex regulation of chromosomally encoded resistance mechanisms.* Clin Microbiol Rev, 2009. **22**(4): p. 582-610.
5. Warrier, T., et al., *Integrated genomics and chemical biology herald an era of sophisticated antibacterial discovery, from defining essential genes to target elucidation.* Cell Chem Biol, 2022. **29**(5): p. 716-729.
6. Johnson, E.O., et al., *Large-scale chemical-genetics yields new M. tuberculosis inhibitor classes.* Nature, 2019. **571**(7763): p. 72-78.
7. Libis, V., et al., *Multiplexed mobilization and expression of biosynthetic gene clusters.* Nat Commun, 2022. **13**(1): p. 5256.
8. Lewis, K., *The Science of Antibiotic Discovery.* Cell, 2020. **181**(1): p. 29-45.
9. Imai, Y., et al., *A new antibiotic selectively kills Gram-negative pathogens.* Nature, 2019. **576**(7787): p. 459-464.
10. Hughes, T.R., et al., *Functional discovery via a compendium of expression profiles.* Cell, 2000. **102**(1): p. 109-26.
11. Hutter, B., et al., *Prediction of mechanisms of action of antibacterial compounds by gene expression profiling.* Antimicrob Agents Chemother, 2004. **48**(8): p. 2838-44.
12. Freiberg, C., H.P. Fischer, and N.A. Brunner, *Discovering the mechanism of action of novel antibacterial agents through transcriptional profiling of conditional mutants.* Antimicrob Agents Chemother, 2005. **49**(2): p. 749-59.
13. Boshoff, H.I., et al., *The transcriptional responses of Mycobacterium tuberculosis to inhibitors of metabolism: novel insights into drug mechanisms of action.* J Biol Chem, 2004. **279**(38): p. 40174-84.
14. O'Rourke, A., et al., *Mechanism-of-Action Classification of Antibiotics by Global Transcriptome Profiling.* Antimicrob Agents Chemother, 2020. **64**(3).
15. Espinoza, J.L., et al., *Predicting antimicrobial mechanism-of-action from transcriptomes: A generalizable explainable artificial intelligence approach.* PLoS Comput Biol, 2021. **17**(3): p. e1008857.
16. Jones, M.B., et al., *Reducing the Bottleneck in Discovery of Novel Antibiotics.* Microb Ecol, 2017. **73**(3): p. 658-667.
17. Murray, J.L., et al., *Intrinsic Antimicrobial Resistance Determinants in the Superbug Pseudomonas aeruginosa.* mBio, 2015. **6**(6): p. e01603-15.
18. Zoffmann, S., et al., *Machine learning-powered antibiotics phenotypic drug discovery.* Sci Rep, 2019. **9**(1): p. 5013.
19. Novak, J.P., R. Sladek, and T.J. Hudson, *Characterization of variability in large-scale gene expression data: implications for study design.* Genomics, 2002. **79**(1): p. 104-13.
20. Planet, P.J., et al., *Systematic analysis of DNA microarray data: ordering and interpreting patterns of gene expression.* Genome Res, 2001. **11**(7): p. 1149-55.
21. Subramanian, A., et al., *A Next Generation Connectivity Map: L1000 Platform and the First 1,000,000 Profiles.* Cell, 2017. **171**(6): p. 1437-1452 e17.
22. Wiegand, I., K. Hilpert, and R.E. Hancock, *Agar and broth dilution methods to determine the minimal inhibitory concentration (MIC) of antimicrobial substances.* Nat Protoc, 2008. **3**(2): p. 163-75.
23. Livermore, D.M., *beta-Lactamases in laboratory and clinical resistance.* Clin Microbiol Rev, 1995. **8**(4): p. 557-84.
24. Munoz-Davila, M.J., *Role of Old Antibiotics in the Era of Antibiotic Resistance. Highlighted Nitrofurantoin for the Treatment of Lower Urinary Tract Infections.* Antibiotics (Basel), 2014. **3**(1): p. 39-48.
25. Guarnieri, M.T., et al., *The Hsp90 inhibitor radicicol interacts with the ATP-binding pocket of bacterial sensor kinase PhoQ.* J Mol Biol, 2008. **379**(1): p. 82-93.
26. Corbett, K.D. and J.M. Berger, *Structural basis for topoisomerase VI inhibition by the anti-Hsp90 drug radicicol.* Nucleic Acids Res, 2006. **34**(15): p. 4269-77.
27. Dutta, R. and M. Inouye, *GHKL, an emergent ATPase/kinase superfamily.* Trends Biochem Sci, 2000. **25**(1): p. 24-8.
28. Verbist, L., *The antimicrobial activity of fusidic acid.* J Antimicrob Chemother, 1990. **25 Suppl B**: p. 1-5.
29. Wehrli, W., *Rifampin: mechanisms of action and resistance.* Rev Infect Dis, 1983. **5 Suppl 3**: p. S407-11.
30. Musialek, M.W. and D. Rybaczek, *Hydroxyurea-The Good, the Bad and the Ugly.* Genes (Basel), 2021. **12**(7).
31. Koc, A., et al., *Hydroxyurea arrests DNA replication by a mechanism that preserves basal dNTP pools.* J Biol Chem, 2004. **279**(1): p. 223-30.
32. Carvalho, C., et al., *Doxorubicin: the good, the bad and the ugly effect.* Curr Med Chem, 2009. **16**(25): p. 3267-85.
33. Gewirtz, D.A., *A critical evaluation of the mechanisms of action proposed for the antitumor effects of the anthracycline antibiotics adriamycin and daunorubicin.* Biochem Pharmacol, 1999. **57**(7): p. 727-41.
34. Minotti, G., et al., *Anthracyclines: molecular advances and pharmacologic developments in antitumor activity and cardiotoxicity.* Pharmacol Rev, 2004. **56**(2): p. 185-229.
35. Pommier, Y., et al., *DNA topoisomerases and their poisoning by anticancer and antibacterial drugs.* Chem Biol, 2010. **17**(5): p. 421-33.
36. Dabrowiak, J.C. and W.T. Bradner, *Platinum antitumour agents.* Prog Med Chem, 1987. **24**: p. 129-58.
37. Nelson, J., et al., *MOSAIC: a chemical-genetic interaction data repository and web resource for exploring chemical modes of action.* Bioinformatics, 2018. **34**(7): p. 1251-1252.

38. Xu, D., et al., *Genome-wide fitness test and mechanism-of-action studies of inhibitory compounds in Candida albicans.* PLoS Pathog, 2007. **3**(6): p. e92.
39. Giaever, G., et al., *Genomic profiling of drug sensitivities via induced haploinsufficiency.* Nat Genet, 1999. **21**(3): p. 278-83.
40. Murkin, A.S., K.A. Manning, and S.A. Kholodar, *Mechanism and inhibition of 1-deoxy-D-xylulose-5-phosphate reductoisomerase.* Bioorg Chem, 2014. **57**: p. 171-185.
41. Rohwer, F. and F. Azam, *Detection of DNA damage in prokaryotes by terminal deoxyribonucleotide transferase-mediated dUTP nick end labeling.* Appl Environ Microbiol, 2000. **66**(3): p. 1001-6.
42. Estrela, C., et al., *Mechanism of action of sodium hypochlorite.* Braz Dent J, 2002. **13**(2): p. 113-7.
43. Franke, R., et al., *Targeting Bacterial Gyrase with Cystobactamid, Fluoroquinolone, and Aminocoumarin Antibiotics Induces Distinct Molecular Signatures in Pseudomonas aeruginosa.* mSystems, 2021. **6**(4): p. e0061021.
44. Poulsen, B.E., et al., *"Multiplexed screen identifies a Pseudomonas aeruginosa-specific small molecule targeting the outer membrane protein OprH and its interaction with LPS".* bioRxiv, 2024: p. 2024.03.16.585348.
45. Deris, Z.Z., et al., *Probing the penetration of antimicrobial polymyxin lipopeptides into gram-negative bacteria.* Bioconjug Chem, 2014. **25**(4): p. 750-60.
46. Steinberg, D.A., et al., *Protegrin-1: a broad-spectrum, rapidly microbicidal peptide with in vivo activity.* Antimicrob Agents Chemother, 1997. **41**(8): p. 1738-42.
47. Zhang, L., et al., *Interactions of bacterial cationic peptide antibiotics with outer and cytoplasmic membranes of Pseudomonas aeruginosa.* Antimicrob Agents Chemother, 2000. **44**(12): p. 3317-21.
48. Cho, H., T. Uehara, and T.G. Bernhardt, *Beta-lactam antibiotics induce a lethal malfunctioning of the bacterial cell wall synthesis machinery.* Cell, 2014. **159**(6): p. 1300-11.
49. Palmer, A.C. and R. Kishony, *Opposing effects of target overexpression reveal drug mechanisms.* Nat Commun, 2014. **5**: p. 4296.
50. Hummels, K.R., et al., *Coordination of bacterial cell wall and outer membrane biosynthesis.* Nature, 2023. **615**(7951): p. 300-304.
51. Li, S., et al., *CRISPRi chemical genetics and comparative genomics identify genes mediating drug potency in Mycobacterium tuberculosis.* Nat Microbiol, 2022. **7**(6): p. 766-779.
52. Meredith, T.C., et al., *Harnessing the power of transposon mutagenesis for antibacterial target identification and evaluation.* Mob Genet Elements, 2012. **2**(4): p. 171-178.
53. Nichols, R.J., et al., *Phenotypic landscape of a bacterial cell.* Cell, 2011. **144**(1): p. 143-56.
54. Geisinger, E., et al., *Antibiotic susceptibility signatures identify potential antimicrobial targets in the Acinetobacter baumannii cell envelope.* Nat Commun, 2020. **11**(1): p. 4522.
55. Lee, D.G., et al., *Genomic analysis reveals that Pseudomonas aeruginosa virulence is combinatorial.* Genome Biol, 2006. **7**(10): p. R90.
56. Stover, C.K., et al., *Complete genome sequence of Pseudomonas aeruginosa PAO1, an opportunistic pathogen.* Nature, 2000. **406**(6799): p. 959-64.
57. Shishkin, A.A., et al., *Simultaneous generation of many RNA-seq libraries in a single reaction.* Nat Methods, 2015. **12**(4): p. 323-5.
58. Zhu, Y.Y., et al., *Reverse transcriptase template switching: a SMART approach for full-length cDNA library construction.* Biotechniques, 2001. **30**(4): p. 892-7.
59. Li, H. and R. Durbin, *Fast and accurate short read alignment with Burrows-Wheeler transform.* Bioinformatics, 2009. **25**(14): p. 1754-60.
60. Abeel, T., et al., *GenomeView: a next-generation genome browser.* Nucleic Acids Res, 2012. **40**(2): p. e12.
61. Love, M.I., W. Huber, and S. Anders, *Moderated estimation of fold change and dispersion for RNA-seq data with DESeq2.* Genome Biol, 2014. **15**(12): p. 550.
62. Becht, E., et al., *Dimensionality reduction for visualizing single-cell data using UMAP.* Nat Biotechnol, 2018.

899 **Figures and Tables**

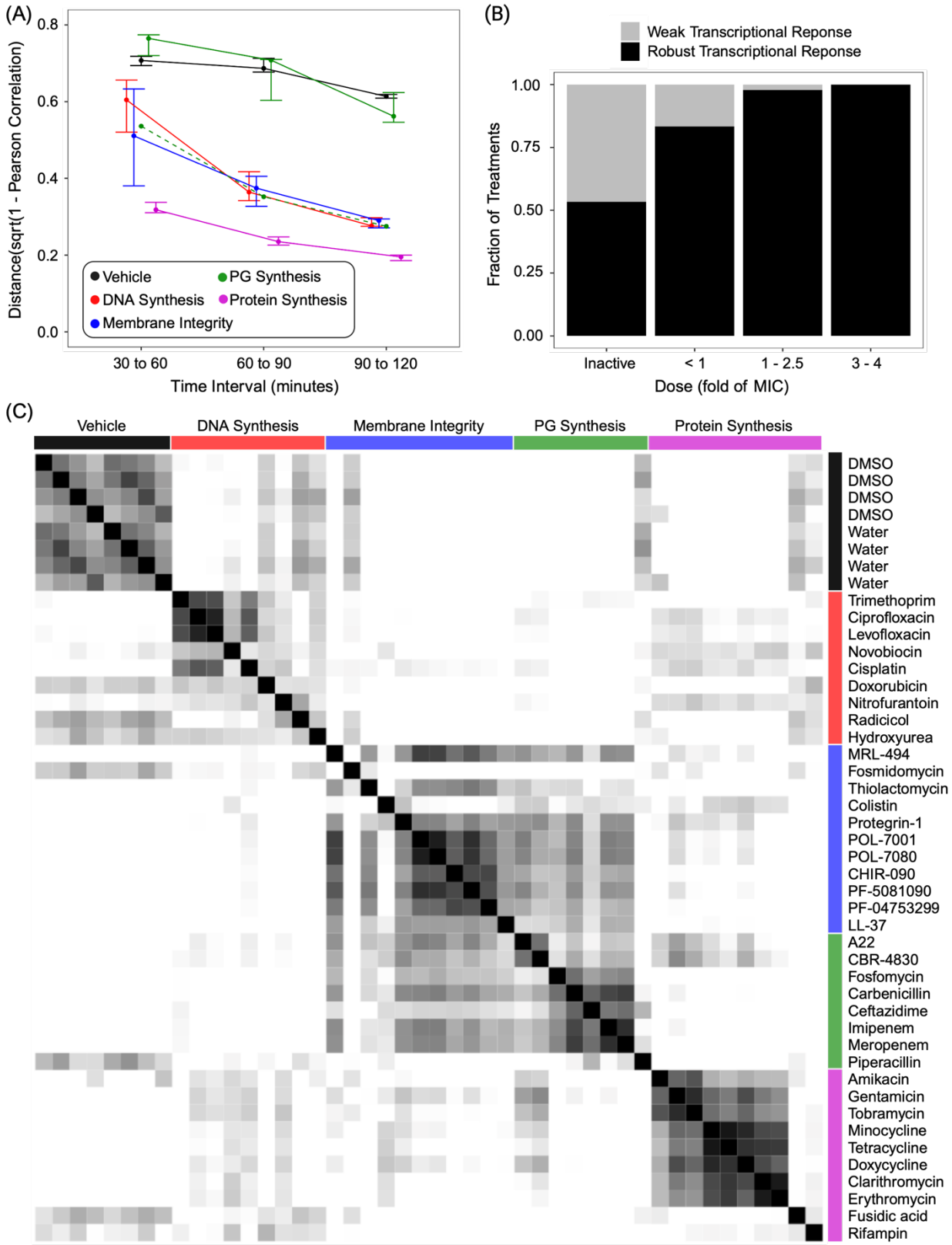

900

901 **Fig. 1.** Gene expression time trial and dose response. (A) Pearson distance between adjacent time points plateau to a
902 stable endpoint for inhibitors of DNA synthesis, membrane integrity, and protein synthesis. Vehicle and inhibitors of
903 peptidoglycan synthesis demonstrate more variability throughout the time course. Imipenem (dotted green line), a
904 peptidoglycan synthesis inhibitor which does not exhibit a significant inoculum effect, also plateau to a stable
905 transcriptional endpoint by 90 minutes. (B) The fraction of all 90-minute treatments having a robust transcriptional
906 response as a function of dose relative to the MIC. Note that a robust transcriptional signature is defined by the
907 differential expression between compound treatment and vehicle control, where at least one gene has an adjusted p-
908 value that is more significant than the minimum adjusted p-value found when comparing PA14 in water versus DMSO
909 control (i.e. $p_{adj} < 10^{-20}$). (C) Heat map shows the Pearson correlations of all 90-minute treatments at the highest dose
910 from both the gene expression time trial and dose response experiments. The rows and columns are sorted based on
911 the MOA of the compounds. All correlation values below zero were set to zero for visualization purposes.

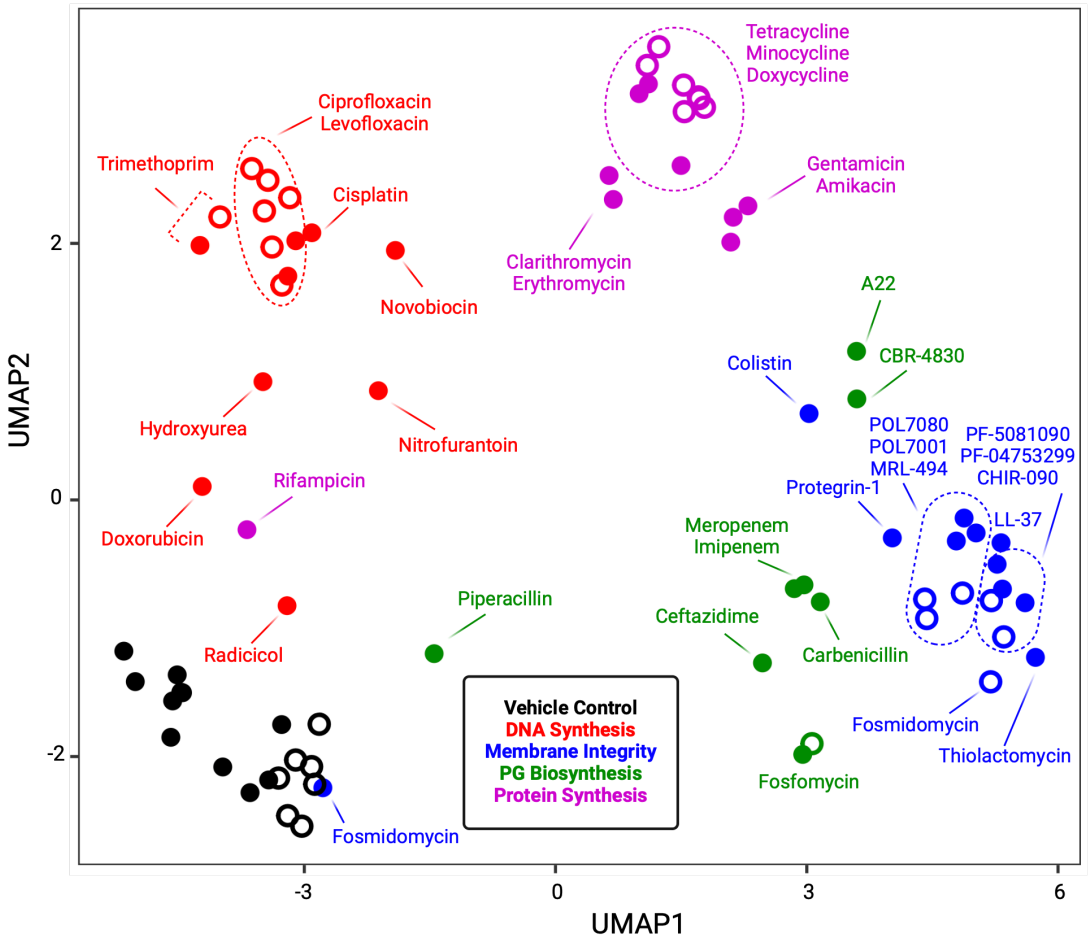

Fig. 2. Treatments of hypersusceptible strains correspond to treatments of wildtype P. aeruginosa. UMAP visualization comprising 90-minute treatments from the gene expression time trial, dose response, and hypomorph experiments. Data includes PA14 and hypomorphic strains treated with vehicle (black) or 39 antimicrobial compounds inhibiting DNA synthesis (red), membrane integrity (blue), peptidoglycan synthesis (green), and protein synthesis (magenta). Closed circles indicate PA14 treatments, whereas open circles indicate treatment of a hypomorphic strain. Antimicrobial compounds with robust activity at the experimental inoculum ($1x10^8$ CFU/mL) group by treatment mechanism agnostic of genetic strain. Protein synthesis inhibitors form sub-groups that separate tetracyclines, macrolides and aminoglycosides. Except for novobiocin, compounds with limited activity PA14, such as fosmidomycin, piperacillin, rifampicin, doxorubicin and hydroxyurea, cluster closer to vehicle.

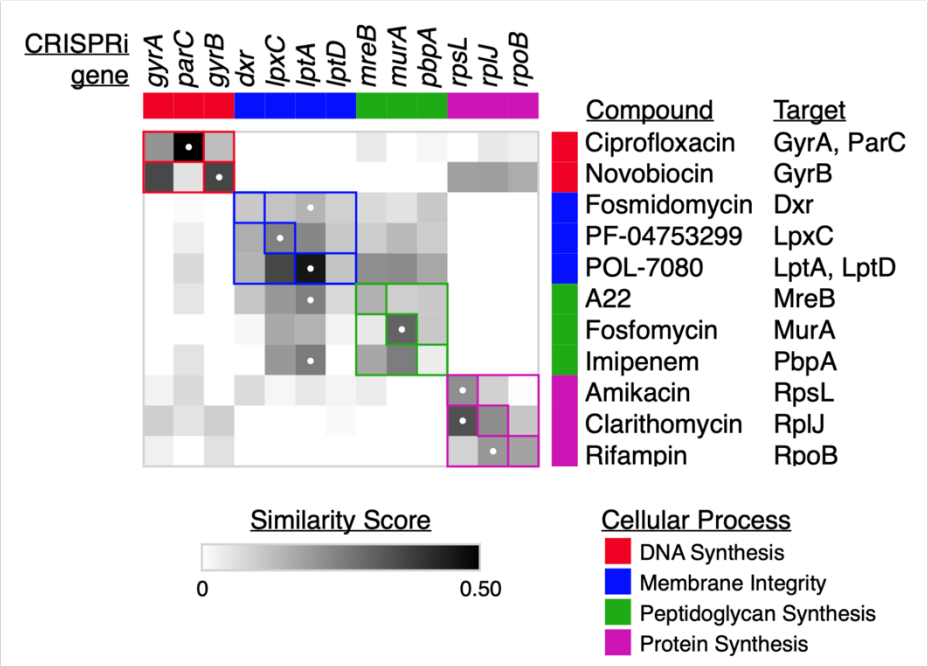

Fig. 3. Similarity scores of CRISPRi reference set to corresponding antimicrobial treatments. Heatmap intensity indicates similarity scores of 90-minute antibiotic treatments when queried against the panel of CRISPRi strains with 0.125% or 0.5% arabinose, the inducer of dCas9 expression. Compound treatments were of PA14 wildtype in all cases except fosmidomycin, which was used to treat the *dxr*-hypomorph, since it did not cause a growth delay of PA14 at the given inoculum. White dots indicate the maximal similarity score for each row. Colored boxes indicate the corresponding target gene(s) or mechanism for each antimicrobial compound.

930 **TABLES:**

Table 1: Summary of the 39 antimicrobial compounds included in the reference set. Antimicrobial compounds used in gene expression time trial are indicated in bold. Antibiotics exhibiting greater or equal to 4-fold shift in MIC at high inoculum are indicated by an asterisk.

MOA	Antibiotic	Class	Target	MIC (μM) Low Inoculum	MIC (μM) High Inoculum
DNA Synthesis	**Ciprofloxacin**	**Fluoroquinolone**	**GyrA/ParC**	**0.25**	**0.25**
	Levofloxacin	**Fluoroquinolone**	**GyrA/ParC**	**1.5**	**1.5**
	Novobiocin	**Novobiocin**	**GyrB**	**>800**	**>800**
	Trimethoprim	**Anti-metabolite**	**DhfR**	**100**	**200**
	Cisplatin	Alkylator	DNA	100	100
	Hydroxyurea	Anti-metabolite	Ribonucleotide reductase	>3200	>3200
	Doxorubicin	Anthracyclines	DNA intercalator	>800	>800
	Radicicol	Macrocycle	HtpG (Hsp90 homolog)	>400	>400
	Nitrofurantoin	Nitrofuran	Protein/DNA damage	>800	>800
Peptidoglycan Synthesis	**Meropenem***	**Carbapenem**	**PBPs**	**1.5**	**6.25**
	Imipenem	**Carbapenem**	**PBPs**	**1.5**	**3.0**
	Ceftazidime*	**Cephalosporin**	**PBPs**	**12.5**	**400**
	Piperacillin*	**Beta Lactam**	**PBPs**	**6.25**	**>400**
	Carbenicillin*	**Beta Lactam**	**PBPs**	**200**	**3200**
	Aztreonam*	**Monobactam**	**PBPs**	**6.25**	**>400**
	Fosfomycin*	**PEP Synthesis**	**MurA**	**250**	**1600**
Protein Synthesis	**Tetracycline**	**Tetracycline**	**30S Ribosome**	**50**	**50**
	Minocycline	**Tetracycline**	**30S Ribosome**	**12.5**	**12.5**
	Erythromycin	**Macrolide**	**50S Ribosome**	**100**	**100**
	Clarithromycin	**Macrolide**	**50S Ribosome**	**100**	**100**
	Amikacin	**Aminoglycoside**	**30S Ribosome**	**1.5**	**3**
	Gentamicin	**Aminoglycoside**	**30S Ribosome**	**3**	**3**
	Doxycycline	Tetracycline	30S Ribosome	50	50
	Tobramycin*	Aminoglycoside	30S Ribosome	1.56	6.25
	Rifampicin	Ansamycins	RpoB	>400	>400
	Fusidic acid	Fusidane	FusA1 (EF-G)	>400	>400
Membrane Integrity	**Colistin***	**Polymyxin**	**Membrane**	**0.78**	**6.25**
	Protegrin-1*	**AMP**	**Membrane**	**2**	**8**
	PF-5081090	**LPS Synthesis**	**LpxC**	**0.4**	**0.8**
	PF-04753299	**LPS Synthesis**	**LpxC**	**0.4**	**0.8**
	LL-37*	AMP	Membrane	12.5	>50
	Fosmidomycin*	Isoprenoid biosynthesis	Dxr	12.5	>400
	POL7001*	LPS Transport	LptD	0.0625	0.500
	POL7080*	LPS Transport	LptD	0.0625	0.125
	CHIR-090*	LPS Synthesis	LpxC	0.78	3.125
	A22*	Actin homolog	MreB	12.5	400
	CBR-4830*	Actin homolog	MreB	15.63	62.5
	MRL-494	OMP folding	BamA	25	25
	Thiolactomycin	Fatty Acid Synthesis	KasA	>400	>400

931

Table 2: Target and MOA prediction of antimicrobial compounds from external and internal datasets using the PerSpecTM approach.

Compound	Predicted Target	Predicted MOA	Similarity Score	Target / MOA PPV	Closest Reference
External Validation using Murray et al. (2015) [17]					
Peroxide	GyrA/ParC	DNA synthesis	0.51	81% / 96%	Ciprofloxacin
Gentamicin	30S RS	Protein synthesis	0.48	79% / 96%	Tobramycin
Ciprofloxacin	GyrA/ParC	DNA synthesis	0.33	61% / 94%	Levofloxacin
Neomycin	30S RS	Protein synthesis	0.33	61% / 94%	Amikacin
Bleach	DNA	DNA synthesis	0.26	NA / NA	Nitrofurantoin
Polymyxin B	LptD	Membrane Integrity	0.26	NA / NA	POL7080
External Validation using Franke et al. (2021) [43]					
Lomefloxacin	GyrA/ParC	DNA synthesis	0.30	62% / 94%	Ciprofloxacin
Ciprofloxacin	GyrA/ParC	DNA synthesis	0.29	62% / 94%	Ciprofloxacin
Levofloxacin	GyrA/ParC	DNA synthesis	0.29	62% / 94%	Ciprofloxacin
Novobiocin	GyrB	DNA synthesis	0.26	58% / 92%	Novobiocin
Internal Validation using screening hits					
PA-0918	LPS	Membrane Integrity	0.74	100% / 100%	Colistin
PA-69180	MreB	Peptidoglycan Synthesis	0.38	68% / 94%	A22
PA-5750	GyrA/ParC	DNA synthesis	0.56	88% / 96%	Ciprofloxacin

932

Table 3: Chemical structures and MIC data for screening hits PA-0918, PA-69180 and PA-5750. The fold decrease in MIC relative to PA14 is shown in parentheses.

Screening Hit	Screening Strain	Chemical Structure	MIC (μM) PA14	MIC (μM) Screening Strain	MIC (μM) PAO397
PA-0918	*lptD*-hypomorph	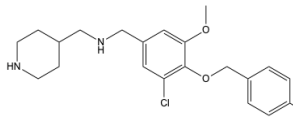	250	125 (2)	31.2 (8)
PA-69180	*oprL*-hypomorph	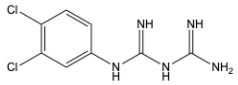	>250	31.2 (>8)	15.6 (>16)
PA-5750	*lptE*-hypomorph	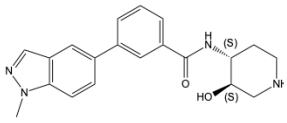	250	125 (2)	<15.6 (>16)

933